Multi-scale performance assessment of Heliosat-4 and LCIM for solar irradiance estimation in Argentina

Anabela Lusi[1,2], Facundo Orte[1], Elian Wolfram[3], Rodrigo Alonso-Suárez[4], and Agustín Laguarda[5]

[1] Departamento de Investigaciones en Láseres y sus Aplicaciones, Instituto de Investigaciones Científicas y Técnicas para la defensa (CITEDEF), Buenos Aires (Argentina)

[2] Universidad Argentina de la Empresa (UADE). Facultad de Ingeniería y Ciencias Exactas (FAIN), Departamento de Agronomía y Ambiente, Buenos Aires (Argentina)

[3] Servicio Meteorológico Nacional (SMN), Buenos Aires (Argentina)

[4] Laboratorio de Energía Solar, Cenur Litoral Norte, Udelar, Salto (Uruguay)

[5] Laboratorio de Energía Solar, Facultad de Ingeniería, Udelar, Montevideo (Uruguay)

Abstract

Accurate estimation of solar resources is essential for the development and deployment of large-scale photovoltaic (PV) systems. Although in situ measurements are the standard for Surface Solar Irradiance (SSI) data, their limited spatial coverage drives the need for reliable spatio-temporal satellite-based models. This study evaluates the performance of two modelling approaches, Heliosat-4 (physical) and a locally tuned Cloud Index Method (CIM, hybrid), for estimating Global Horizontal Irradiance (GHI) over the Pampa Húmeda region of Argentina. The analysis builds on previous studies by incorporating two additional monitoring sites from the Saver-Net network and evaluating the model performance at different temporal resolutions (10 min, 15 min and hourly). The preliminary validation results showed that the CIM based on GOES imagery outperformed the Heliosat-4 based on Meteosat Second Generation (MSG) imagery at all time scales evaluated, with better performance metrics and higher correlation with SSI.

Keywords: GHI, satellite-based models, solar resource estimation performance

1. Introduction

Accurate solar radiation models are essential for the reliable assessment of large-scale solar energy potential. Understanding local solar radiation conditions is critical for the proper design of solar photovoltaic (PV) systems and building energy strategies (Li and Lam, 2000; Wong and Chow, 2001). In addition, accurate solar radiation data play a key role in the economic assessment of PV projects, since the uncertainty associated with these measurements is considered the main financial risk factor in PV systems (McMahan et al., 2013; Schnitzer et al., 2012).

Although the most direct way to understand these dynamics is through in-situ measurements, obtaining Surface Solar Irradiance (SSI) data at every location remains challenging owing to the significant cost of both equipment and human resources. Therefore, solar radiation models based satellite imagery have emerged as practical alternatives, provided that their outputs are validated against high-quality SSI measurements from well-instrumented reference sites.

Satellite-based models offer a reliable alternative for estimating SSI over broad regions. Depending on the nature of the input information, satellite-based models can be classified into three main categories: empirical (Cano et al., 1986; Tarpley, 1979), physical (Gautier et al., 1980; Qu et al., 2017; Raschke and Preuss, 1979), and hybrid (or semi-empirical) (Perez et al., 2002; Rigollier et al., 2004).

Since clouds are the main factor influencing SSI, and usually exhibit significant short-term variability, high-rate geostationary satellite images are generally used to provide this information. The region of interest in this study is the Pampa Húmeda of Argentina, southern South America. This area is covered by two geostationary satellites,

GOES-16 (part of NOAA's GOES-East system) and Meteosat Second Generation (MSG), operated by EUMETSAT. Due to their respective positions in geostationary orbit, each satellite observes an area with different viewing angles and spatial resolutions.

One widely used physical model is Heliosat-4, which estimates the downwelling shortwave irradiance received at ground level under all-sky conditions. It provides global irradiance as well as its direct and diffuse components on a horizontal plane, and direct irradiance on a plane normal to the sun's rays (Qu et al., 2017). Heliosat-4 primarily uses data from the MSG satellites for cloud properties.

On the other hand, a common hybrid modeling approach is to use a physical clear-sky model modulated by a satellite-derived cloud index to estimate solar irradiance under all-sky conditions. These models are collectively referred to as Cloud Index Methods (CIM). Examples of such methods can be found in Beyer et al. (1996) and Rigollier et al. (2004).

Laguarda et al. (2020) evaluated the performance of several solar irradiance models in the Pampa Húmeda region (southeastern South America), including the Heliosat-4 method and two locally adjusted CIM. Their analysis, which used hourly ground measurements from 10 sites, showed that CIMs using GOES-East imagery outperformed other methods. The better performance of the CIMs was attributed not only to the local parameter adjustment but also to the more favorable viewing angle of the GOES-East satellite. The adjusted parameters were consistent across the region, supporting their applicability beyond the original training sites.

Building on this work, the present study focuses exclusively on the Heliosat-4 physical model and the hybrid CIM, using updated data and extending the analysis to two additional sites in the same climatic region that are part of the Saver-Net solar radiation monitoring network in Argentina (Orte et al., 2022). For the CIM model, the same locally tuned parameters proposed by Laguarda et al. (2020) are adopted given their proven robustness. In contrast to previous studies using hourly resolution, this study evaluates model performance using 10-minute, 15-minute and 1-hour temporal resolutions. The aim is to assess the accuracy of both models under hourly and sub-hourly temporal resolution and validate their applicability in new locations within Pampa Húmeda, contributing to the regional understanding of satellite-based solar irradiance modeling and its typical uncertainty.

2. Ground measurements

The Argentine Total Solar Irradiance Monitoring Network, established as part of the Saver-Net project, consists of eight stations between approximately 26ºS and 52ºS, distributed throughout the country. Its main objective is to generate reliable data for basic and applied research on atmospheric monitoring from the Earth's surface. The Saver-Net network is equipped with various remote sensing instruments, such as broadband and narrow band radiometers, sun photometers, lidar systems, DOAS spectrometers, sky cameras, and conventional weather stations. It is operated by the Argentine Servicio Meteorológico Nacional (SMN, https://www.smn.gob.ar/) and DEILAP (CITEDEF-UNIDEF, https://unidef.conicet.gov.ar/deilap/) (Orte et al., 2022).

From the eight stations comprising the Saver-Net network, this study focused on two sites: Pilar, Córdoba (PIL, 31.68 °S, 63.87 °W, 330 m a.s.l.) and Villa Martelli, Buenos Aires (VMA, 34.58 °S, 58.48 °W, 25 m a.s.l.). Both sites are equipped with Kipp&Zonen CMP21 pyranometers, which provide 1-minute Global Horizontal Irradiance (GHI) data. The typical uncertainty reported for these instruments is ±2% for daily totals (OTT HydroMet, 2023). The analysis was based on the data collected between 2018 and 2022. These locations are situated within the South American ecoregion known as Pampa Húmeda, which is characterized by homogeneous temperate grassland plains and intense agricultural activity. This region spans most of Argentina's central-eastern territory, as well as Uruguay and southern Brazil (see Figure 1). According to the Köppen-Geiger climate classification (Peel et al., 2007), the Pampa Húmeda is predominantly classified as Cfa, denoting a humid subtropical climate with hot, humid summers and mild winters. Precipitation is abundant, especially near coastal areas, but gradually decreases inland, leading to drier winter conditions as the distance from the Atlantic Ocean increases.

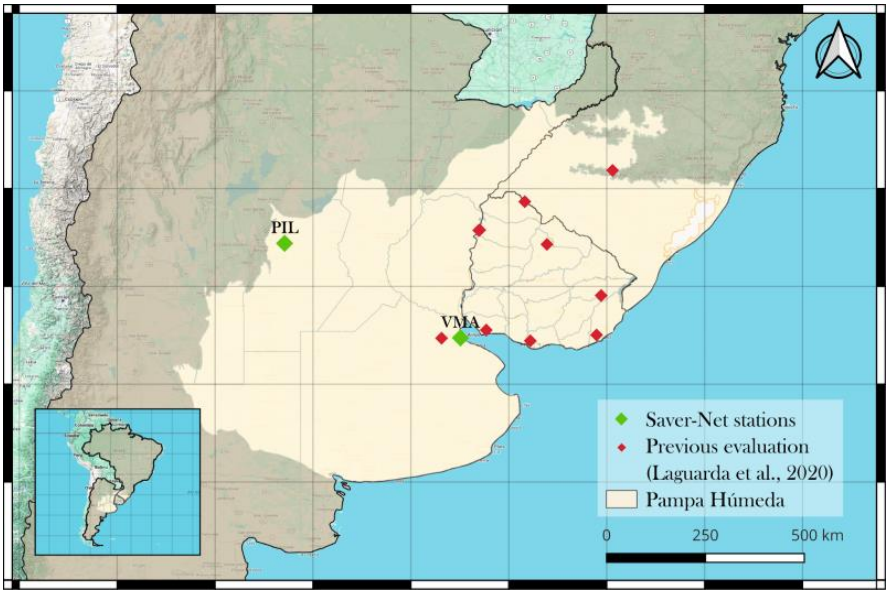

Figure 1: Geographic distribution of the evaluation sites. Red diamonds indicate locations previously evaluated in Laguarda et al. (2020), while green diamonds represent the two Saver-Net stations assessed in this study (PIL and VMA). The beige area indicates the Pampa Húmeda region.

The 10-minute, 15-minute and 1-hourly averages were calculated from the original 1-minute measurements recorded at each site. To ensure data quality, a series of quality control (QC) filters were applied to minute-level measurements prior to aggregation. The first filter excluded measurements taken at solar elevations below 7° because the relative error is known to be higher when the sun is close to the horizon. The second filter removes values with a clearness index (kt) greater than 1.35, which may indicate sensor anomalies (Geuder et al., 2015; Gueymard, 2017). The final filter targeted systematic errors such as shading effects.

3. Models and performance metrics

3.1. Models description

The model Heliosat-4 relies on a fast yet accurate approximation of the libRadtran radiative transfer model (RTM) and incorporates cloud information derived from MSG (located at 0° longitude in a geostationary orbit above the Earth's equator) satellite images. It uses the APOLLO/SEV methodology for cloud retrieval and incorporates other atmospheric input data such as aerosol properties, total column water vapor, and ozone concentrations from the CAMS reanalysis database, as well as daily surface albedo estimates from the MODIS instrument onboard the Terra and Aqua low Earth orbit satellites. These data are publicly available at https://www.soda-pro.com/web-services/radiation/cams-radiation-service. Heliosat-4 estimates are available at both 1-minute, 15-minute and 1-hour resolutions; therefore, to allow comparison at the 10-minute scale, the 1-minute estimates will be downloaded and averaged accordingly.

As mentioned above, the CIMs have the common structure of a clear-sky model modulated by an attenuation factor that considers the effect of clouds. This modulating factor is based on the cloudiness index derived from the satellite imagery. The general structure of the model can be expressed as:

$$GHI = GHI_{CC} x F(\eta) \qquad \text{(eq. 1)}$$

where GHI is the estimated global horizontal irradiance under all-sky conditions at the given timescale, GHI_{CC} is the estimated clear-sky global irradiance on a horizontal plane, and $F(\eta)$ represents the cloud index attenuation function with the η being the cloudiness index. The formulation of $F(\eta)$ is detailed below.

$$F(\eta) = a + b(1 - \eta) \qquad \text{(eq. 2)}$$

where a and b are empirical coefficients. These parameters were originally derived by Laguarda (2021), with values adjusted for the Pampa Húmeda region, optimized for a fixed cell size and hourly frequency.

The cloudiness index (η), originally proposed by Cano et al. (1986), is a dimensionless parameter ranging from 0 (clear-sky conditions) to 1 (full cloud cover). It is derived from the planetary reflectance (R) observed by satellites,

which is normalized for each pixel in the satellite image using a dynamic range defined by minimum and maximum values. These reference values vary depending on the day of the year and the time of day. The η is computed as follows:

$$\eta = \frac{R - R_0}{R_{MAX} - R_0} = \frac{F_R - F_{R0}}{R_{MAX} cos(\theta_z) - F_{RO}} \qquad \text{(eq. 3)}$$

Here, $R = F_R / cos\ (\theta_z)$, where θ_z is the solar zenith angle. The reflectance factor F_R is obtained from the visible channel of the GOES-East geostationary satellite (located at 75ºW longitude). F_{R0} (and thus R_0) represents the reflectance of a cloud-free pixel and is referred to as the background brightness. This value is determined through a parametrization that depends on the relative position between the satellite and the Sun, using an iterative procedure originally proposed by Tarpley (1979) and later adapted by Alonso-Suárez (2017). Finally, R_{MAX} corresponds to a constant value that represents overcast sky conditions. This maximum value was set for each station so that only 0.2% of samples are clipped. The values obtained range from 0.90 to 1.00, which is consistent with the findings of Laguarda et al. (2018).

This model was developed by the Laboratorio de Energía Solar (LES), Universidad de la República, Uruguay, specifically for the Pampa Húmeda region. The model with these considerations and adjusted parameters is referred to as LCIM (with "L" standing for LES) and has proven to be among the most accurate for this climatic region as it was trained specifically for these conditions.

The clear-sky model used in the CIM can vary. In this study, we employed the McClear model (Lefèvre et al., 2013) which showed good performance in a previous study on the same SAVER-Net sites (Lusi et al., 2023). Since the GOES satellite provides data at a 10-minute frequency, we applied linear interpolation to obtain 15-minute values, and calculated averages to obtain hourly values. These temporal adjustments were made to enable consistent comparison with Heliosat-4 estimates.

3.2. Metrics

The statistical error indicators used in this work are a subset of those suggested for detailed validation studies (Gueymard, 2014) and consist of RMSD, MBD, and MAD, defined as:

$$RMSD = \left[\frac{1}{N}\sum_i^N e_i^2\right]^{\frac{1}{2}} \qquad \text{(eq. 4)}$$

$$MBD = \frac{1}{N}\sum_i^N e_i \qquad \text{(eq. 5)}$$

$$MAD = \frac{\sum_i^N |e_i|}{N} \qquad \text{(eq. 6)}$$

where N is the number of pairs of measurements (y_i) and estimates ($\hat{y}_i$), and e_i are the residuals $\hat{y}_i - y_i$. These indicators can be expressed in relative terms ($rRMSD$, $rMBD$, and $rMAD$) as a percentage of the mean of the measurements $\langle y_i \rangle$.

In addition to $RMSD$, MBD, and MAD, the coefficient of determination (R^2) is also used as a statistical indicator. R^2 quantifies the proportion of variance in the measured data that is explained by the estimates, providing insight into the accuracy and predictive capability of the model.

4. Results and discussion

The LCIM model was tested at 18 different spatial resolutions to assess its sensitivity to grid size and spatial representation. Each configuration employed a square grid in latitude and longitude with resolutions expressed in decimal degrees. The tested grid were: 0.025º, 0.035º, 0.050º, 0.075º, 0100º, 0.125º, 0.150º, 0.200º, 0.300º, 0.350º, 0.400º, 0.450º, 0.500º, 0.600º, 0.700º, 0.800º, and 0.900º. These values encompass a wide range of spatial scales, from fine-resolution grids capable of capturing detailed local cloud variability to coarser grids representing broader regional patterns.

The results obtained for each resolution are shown in Figure 2. The curve represents the spatial average of the performance (rRMSD) over each station as a function of cell size. The corresponding performance metrics are summarized in Table 1.

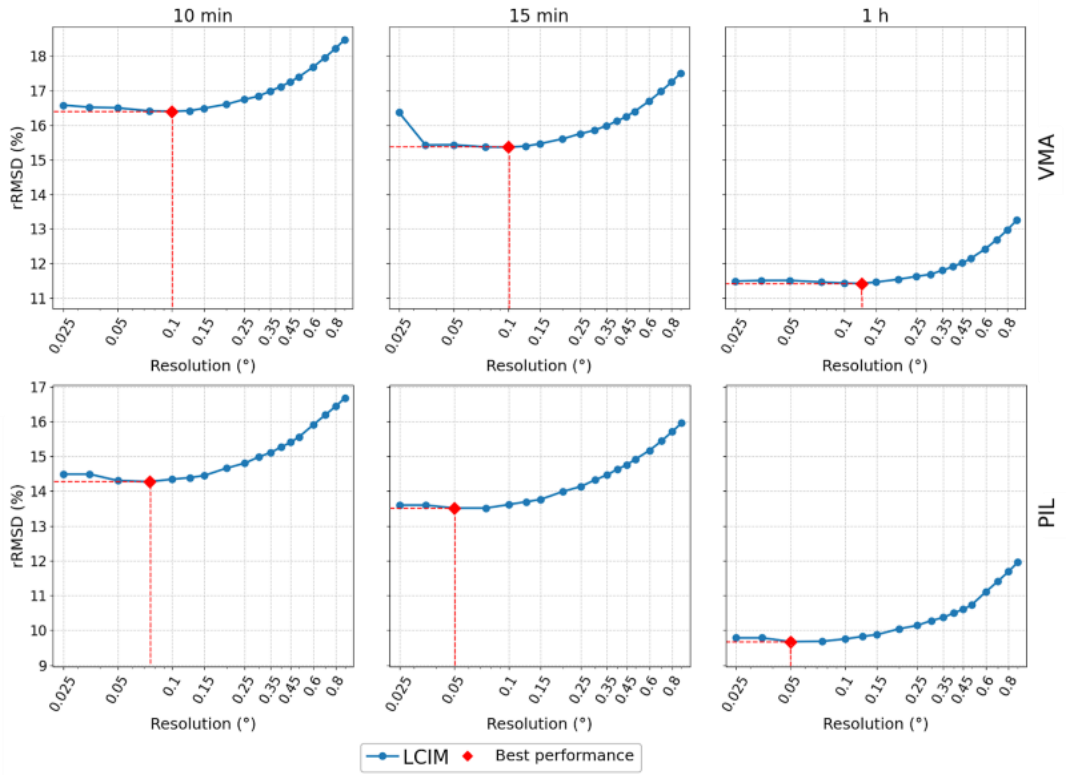

Figure 2: rRMSD values for the LCIM model with different spatial resolutions. Results are shown for three temporal resolutions (10 min, 15 min, and 1 h) and for two sites: VMA (top) and PIL (bottom). Red diamonds indicate the best performances.

Table 1: Performance assessment for the different satellite-based models and temporal resolutions.

		LCIM				Heliosat-4		
		rRMSD (%)	rMAD (%)	rMBD (%)	Resolution (°)	rRMSD (%)	rMAD (%)	rMBD (%)
VMA	10 min	16.4	11.1	2.4	0.100	21.3	12.7	-5.0
	15 min	15.4	10.5	2.5	0.100	20.2	12.2	-4.9
	1 h	11.4	8.3	2.1	0.125	15.9	9.9	-4.8
PIL	10 min	14.3	8.8	2.3	0.075	22.2	13.7	-4.7
	15 min	13.5	8.4	2.3	0.050	21.4	13.3	-4.7
	1 h	9.7	6.6	2.2	0.050	17.5	11.0	-4.0

As shown in Figure 2, at the VMA site, a resolution of 0.100° yielded the best performance for high-frequency data, with rRMSD values of 16.4% (10 min) and 15.4% (15 min). For hourly data, a slightly higher resolution of 0.125° produced the lowest error (11.4% rRMSD). At the PIL site, the optimal resolution for sub-hourly data was 0.075° and 0.050º, achieving rRMSD values of 14.3% (10 min) and 13.5% (15 min), respectively. For hourly data, a resolution of 0.050° provided the best performance, with a notably low rRMSD of 9.7%. These rRMSD values are consistent with the performance metrics typically reported in studies across the region.

The rRMSD was sensitive to the grid resolution, showing a clear tendency to increase as the grid becames coarser (typically above 0.15°). However, at finer resolutions, the behavior is relatively stable (except for PIL at 15 min) until reaching a minimum rRMSD value, beyond which the error rises again. The difference between the optimal and extreme grid sizes (e.g., 0.025° and 0.900°) underscores the importance of spatial optimization. For instance, at the VMA site at 10 min, the rRMSD increases from 16.4% to over 18%, depending solely on the chosen grid size.

When comparing the performance between models, at the VMA site, the Heliosat-4 model showed rRMSD values of 21.3%, 20.2%, and 15.9% at 10 min, 15 min, and 1 h resolution, respectively. At the PIL site, the results were 22.2%, 21.4%, and 17.5% at 10 min, 15 min, and 1 h, respectively. These results are consistent with those of

previous studies conducted in the region. Figure 3 illustrates the scatter plots of the measured versus estimated GHI for both models and time resolutions. A clear improvement was observed when transitioning from Heliosat-4 (upper panels) to LCIM (lower panels), as reflected in both the tighter clustering of points around the 1:1 line and the increase in the R^2.

The lower performance of Heliosat-4 at the PIL site compared to VMA is consistent with the larger viewing angle of the MSG satellite, which increases the atmospheric path length and amplifies the parallax effects. As the viewing angle exceeds approximately 60° (the recommended maximum view angle indicated by the Heliosat-4 manual), uncertainties in cloud optical properties, and consequently in the derived irradiance, become more pronounced. It is also worth noting that Heliosat-4 estimates were used here outside the model's recommended geographical coverage, and their performance was therefore affected by the large viewing angle of the MSG satellite over this region. In contrast, the LCIM, based on GOES-East imagery, benefits from a more favourable viewing geometry and the inclusion of locally tuned parameters, resulting in higher accuracy and lower bias, even at sub-hourly scales. Overall, the improvement in rRMSD and R^2 from Heliosat-4 to LCIM supports the advantage of using regionally adjusted hybrid approaches for solar resource estimation in the Pampa Húmeda region.

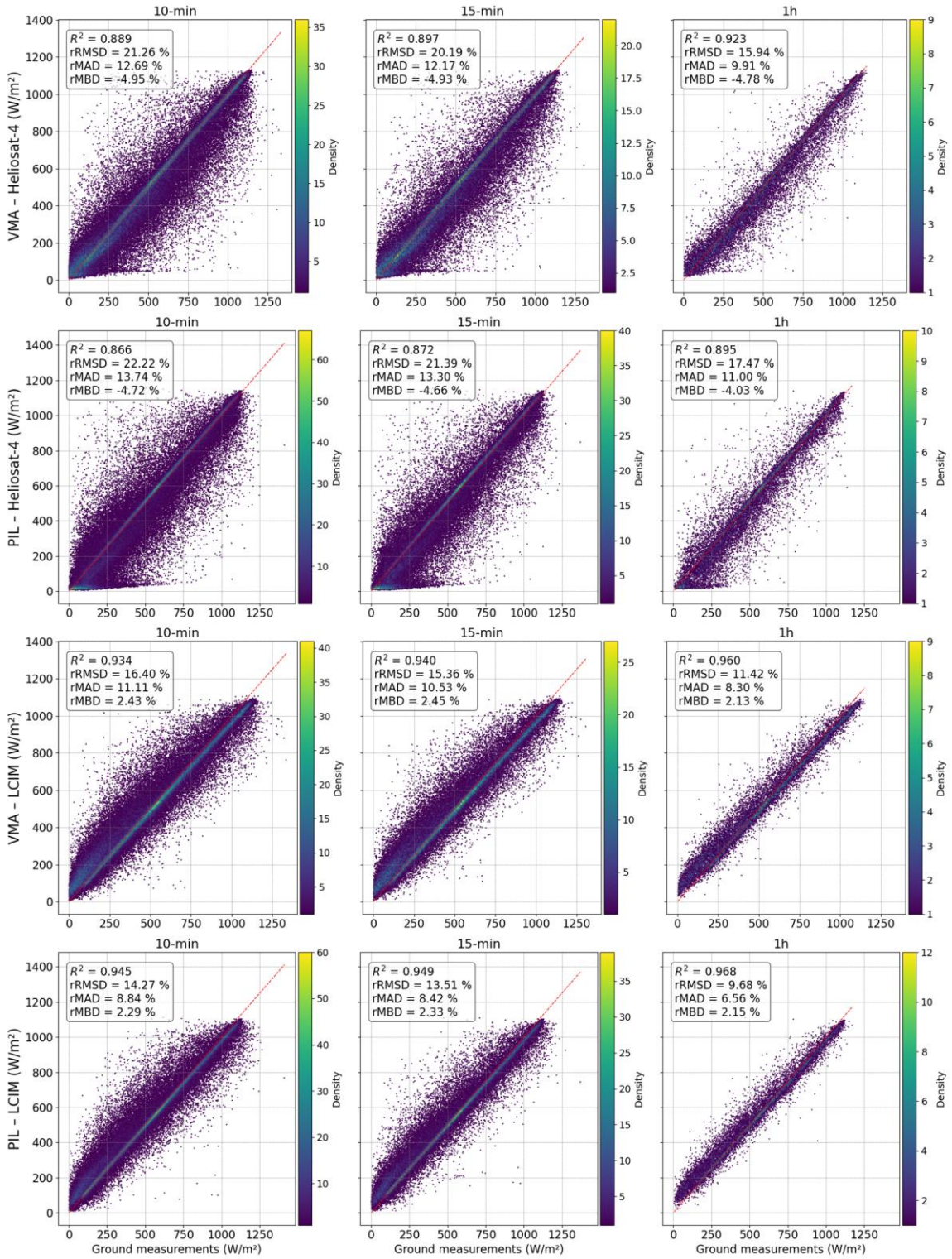

Figure 3: Comparison between ground measurements and satellite-derived estimates from the Heliosat-4 (top) and LCIM (bottom) models for VMA and PIL sites. Each row corresponds to a different site, while the columns represent temporal averaging intervals of 10 minutes, 15 minutes, and 1 hour.

On the other hand, as expected, the performance of both models improved as the temporal resolution increased, particularly when changing from sub-hourly to hourly intervals. In all cases, the LCIM achieved superior performance. This comparative analysis highlights the importance of regionally calibrated models and appropriate satellite and resolution selection for satellite-based solar irradiance estimation.

5. Conclusions

Two types of satellite-based models for estimating SSI were assessed at the 10-minute, 15-minute, and hourly temporal resolutions, incorporating two additional sites compared to previous research within the same climatic region of the Pampa Húmeda. The main difference between the models lies in the satellite data used, Heliosat-4 relies on MSG, whereas LCIM is based on GOES-East data.

The results showed that the LCIM, which combines the McClear clear-sky model with a locally tuned cloud index, outperformed the Heliosat-4 physical model at all temporal scales and provided performance metrics consistent with reports from the same region. The improved performance of LCIM was particularly evident in the reduction of rRMSD and the increase in R^2, demonstrating the benefits of using regionally calibrated hybrid models. In contrast, the lower accuracy of Heliosat-4 was largely attributed to the unfavorable viewing geometry of the MSG over Argentina, which amplifies parallax and atmospheric path-length effects.

Both models exhibited improved accuracy as the temporal resolution became coarser, highlighting the smoothing effect of temporal averaging on the short-term variability and cloud dynamics. Additionally, the sensitivity analysis of LCIM to spatial resolution indicated an optimal grid size between 0.05° and 0.125°, beyond which the performance deteriorated.

Overall, this study confirms the robustness of the locally calibrated CIM across multiple sites and timescales in the Pampa Húmeda. These results emphasize the relevance of regional calibration and appropriate satellite selection for accurate solar resource model validation in southern South America, contributing to the evaluation and consolidation of satellite-based irradiance models in Argentina.

As a future line of work, the coefficients a and b of the cloud index attenuation function $F(\eta)$ could be recalculated and adjusted as a function of both spatial resolution and temporal frequency to further improve the model performance.

6. Acknowledgments

The authors would like to express their gratitude to the Japan International Cooperation Agency (JICA) and Japan Science and Technology Agency (JST) for their financial support for the Saver-Net project. Additionally, we thank institutions SMN and DEILAP (CITEDEF-UNIDEF), for operating and maintaining the Saver-Net network.

Anabela Lusi is a graduate student in the Environmental and Health Applied Sciences Doctoral Program (DCAAS) at National University of the Center of Buenos Aires Province (UNCPBA), Argentina.

7. References

Alonso-Suárez, R., 2017. Estimación del recurso solar en Uruguay mediante imágenes satelitales. Universidad de la República, Uruguay.

Beyer, H.G., Costanzo, C., Heinemann, D., 1996. Modifications of the Heliosat procedure for irradiance estimates from satellite images. Sol. Energy 56, 207–212. https://doi.org/10.1016/0038-092X(95)00092-6

Cano, D., Monget, J.M., Albuisson, M., Guillard, H., Regas, N., Wald, L., 1986. A method for the determination of the global solar radiation from meteorological satellite data. Sol. Energy 37, 31–39. https://doi.org/10.1016/0038-092X(86)90104-0

Gautier, C., Diak, G., Masse, S., 1980. A Simple Physical Model to Estimate Incident Solar Radiation at the Surface from GOES Satellite Data. J. Appl. Meteorol. 1962-1982 19, 1005–1012.

Geuder, N., Wolfertstetter, F., Wilbert, S., Schüler, D., Affolter, R., Kraas, B., Lüpfert, E., Espinar, B., 2015. Screening and Flagging of Solar Irradiation and Ancillary Meteorological Data. Energy Procedia, International Conference on Concentrating Solar Power and Chemical Energy Systems, SolarPACES 2014 69, 1989–1998. https://doi.org/10.1016/j.egypro.2015.03.205

Gueymard, C.A., 2017. Cloud and albedo enhancement impacts on solar irradiance using high-frequency

measurements from thermopile and photodiode radiometers. Part 1: Impacts on global horizontal irradiance. Sol. Energy 153, 755–765. https://doi.org/10.1016/j.solener.2017.05.004

Gueymard, C.A., 2014. A review of validation methodologies and statistical performance indicators for modeled solar radiation data: Towards a better bankability of solar projects. Renew. Sustain. Energy Rev. 39, 1024–1034.

Laguarda, A., 2021. Modelado de la irradiancia solar sobre la superficie terrestre: modelos físicos e híbridos utilizando información satelital sobre la Pampa Húmeda. Universidad de la República, Uruguay.

Laguarda, A., Abal, G., Alonso-Suarez, R., 2018. MODELO SEMI-EMPÍRICO SIMPLE DE IRRADIACIÓN SOLAR GLOBAL A PARTIR DE IMÁGENES SATELITALES GOES. An. Congr. Bras. Energ. Sol. - CBENS. https://doi.org/10.59627/cbens.2018.707

Laguarda, A., Giacosa, G., Alonso-Suárez, R., Abal, G., 2020. Performance of the site-adapted CAMS database and locally adjusted cloud index models for estimating global solar horizontal irradiation over the Pampa Húmeda. Sol. Energy 199, 295–307. https://doi.org/10.1016/j.solener.2020.02.005

Lefèvre, M., Oumbe, A., Blanc, P., Espinar, B., Gschwind, B., Qu, Z., Wald, L., Schroedter-Homscheidt, M., Hoyer-Klick, C., Arola, A., Benedetti, A., Kaiser, J.W., Morcrette, J.-J., 2013. McClear: a new model estimating downwelling solar radiation at ground level in clear-sky conditions. Atmospheric Meas. Tech. 6, 2403–2418. https://doi.org/10.5194/amt-6-2403-2013

Li, D.H.W., Lam, J.C., 2000. Solar heat gain factors and the implications to building designs in subtropical regions. Energy Build. 32, 47–55. https://doi.org/10.1016/S0378-7788(99)00035-3

Lusi, A.R., Orte, F., Suárez, R.A., D'Elía, R., Wolfram, E., 2023. EVALUACIÓN DE LOS MODELOS DE RADIACIÓN SOLAR GLOBAL HELIOSAT-4 Y MCCLEAR EN DOS SITIOS DE ARGENTINA. An. AFA 34, 76–81.

McMahan, A.C., Grover, C.N., Vignola, F.E., 2013. Chapter 4 - Evaluation of Resource Risk in Solar-Project Financing, in: Kleissl, J. (Ed.), Solar Energy Forecasting and Resource Assessment. Academic Press, Boston, pp. 81–95. https://doi.org/10.1016/B978-0-12-397177-7.00004-8

Orte, F., Wolfram, E., Luccini, E., D'Elia, R., Lusi, A., Pallotta, J., Nollas, F., Carmona, F., Papandrea, S., Cabezas, M.D., Benítez, G.C., Mizuno, A., 2022. Red de Monitoreo de la Irradiancia Solar UV-Total en Argentina "Saver-Net." Meteorológica 47. https://doi.org/10.24215/1850468Xe016

OTT HydroMet, 2023. CMP Series Pyranometers, Operational Manual.

Peel, M., Finlayson, B., Mcmahon, T., 2007. Updated World Map of the Koppen-Geiger Climate Classification. Hydrol. Earth Syst. Sci. Discuss. 4. https://doi.org/10.5194/hess-11-1633-2007

Perez, R., Ineichen, P., Moore, K., Kmiecik, M., Chain, C., George, R., Vignola, F., 2002. A new operational model for satellite-derived irradiances: description and validation. Sol. Energy 73, 307–317. https://doi.org/10.1016/S0038-092X(02)00122-6

Qu, Z., Oumbe, A., Blanc, P., Espinar, B., Gesell, G., Gschwind, B., Klüser, L., Lefèvre, M., Saboret, L., Schroedter-Homscheidt, M., Wald, L., 2017. Fast radiative transfer parameterisation for assessing the surface solar irradiance: The Heliosat-4 method. Meteorol. Z. 26, 33–57. https://doi.org/10.1127/metz/2016/0781

Raschke, E., Preuss, H.J., 1979. The determination of the solar radiation budget at the Earth's surface from satellite measurements. Meteorol. Rundsch. 32, 18–28.

Rigollier, C., Lefèvre, M., Wald, L., 2004. The method Heliosat-2 for deriving shortwave solar radiation from satellite images. Sol. Energy 77, 159–169. https://doi.org/10.1016/j.solener.2004.04.017

Schnitzer, M., Thuman, C., Johnson, P., 2012. The impact of solar uncertainty on project financeability: mitigating energy risk through on-site monitoring. Proc. Am. Sol. Energy Soc. ASES 1–5.

Tarpley, J.D., 1979. Estimating Incident Solar Radiation at the Surface from Geostationary Satellite Data.

Wong, L.T., Chow, W.K., 2001. Solar radiation model. Appl. Energy 69, 191–224. https://doi.org/10.1016/S0306-2619(01)00012-5